Influence of slant of objective on image formation in optical microscopes

Jiangang Wang* and Rainer Köning

Physikalisch-Technische Bundesanstalt Braunschweig, Bundesallee 100, 38116 Braunschweig, Germany

Received November 8, 2007

A microscope image formation model based on scalar diffraction and Fourier optics has been developed, which takes a slant angle between the optical axis and the observed surface into account. The theoretical investigations of the imaging of line structures using this model show that reflection type microscopes are much stronger influenced by the slant angle than transmission type microscopes. In addition, the slant angle changes the image contrast and the image shape of a line structure, especially its edge. The larger the slant angle, the stronger the decrease of the image contrast, and the less steep the edge slope in both types of microscopes. Furthermore, the larger the numerical aperture of the objective, the less the effect of the slant angle on the line image shape.

OCIS codes: 120.3940, 180.0180, 110.2990.

doi: 10.3788/COL20080608.0603.

Linewidth measurements are important in semiconductor industries. Microscope image formation models are needed to understand the images of line structures and find a suitable edge setting criterion. Although theories of the image formation of optical microscopes based on scalar diffraction and Fourier optics are widely in use, there are still some problems in modelling the image formation of submicron or micron structures due to the complex influence of the operating conditions, such as aberrations, misalignment, illumination evenness and its coherence etc.[1,2] Images of line structures were already analyzed in the presence of aberrations and coherence, incoherence and partial coherence illumination[3−6]. The mainly used method was derived from Hopkins' theory of partially coherent imaging, which uses concepts of the effective source and transmission cross coefficients (TCC)[7,8]. Misalignment is an often-met problem. Under perfect condition, the observed surface is orthogonal to the optical axis and coincides with the focal plane, and the photo detector is also orthogonal to the optical axis and is located exactly in the image plane. But in practice, the observed surface always exhibits a slant angle with the focal plane. To our knowledge, the effect of such a slant angle on image formation of optical microscopes has not been analyzed yet. In this letter, a microscope imaging model is developed to discuss this effect considering the slant angle and objective numerical apertures (NAs) in transmission type and reflection type microscopes.

The notation and treatment of the image formation given by Kirk were closely followed[9,10]. The one-dimensional (1D) imaging theory of a single line is developed for simplification. And the slant direction is vertical to the orientation of line structure. We also assume that the line structure center is on the optic axis. Figure 1 shows a Köhler illumination set up. The light emanates from one point P on the entrance pupil of the condenser and passes through the condenser to produce a collimated beam and thus illuminates the object with a planar wavefront by an angle θ with the optical axis z. There is a slant angle α between the object surface $f(x')$ and the focal plane. The collimated beam is then diffracted by an angle ψ with the optical axis. The phase delay between the light rays 1 and 2 at a point x' in the object plane will be given by (see Fig. 2)

$$\phi(x') = x' \frac{2\pi}{\lambda} [\sin(\theta - \alpha) - \sin(\psi - \alpha)] \quad (1)$$

for the transmission type microscope and

$$\phi(x') = x' \frac{2\pi}{\lambda} [\sin(\theta + \alpha) - \sin(\psi - \alpha)] \quad (2)$$

for the reflection type microscope. The superposition of all the elementary waves from the object will thus lead to

$$g(\psi, \theta, \alpha) = \int_{-\infty}^{\infty} f(x') \exp(i\phi(x')) \mathrm{d}x', \quad (3)$$

where $g(\psi, \theta, \alpha)$ represents the far-field diffraction pattern of the object and also the diffraction pattern in the back focal plane of the objective. Using $k = 2\pi/\lambda$, Eq. (3)

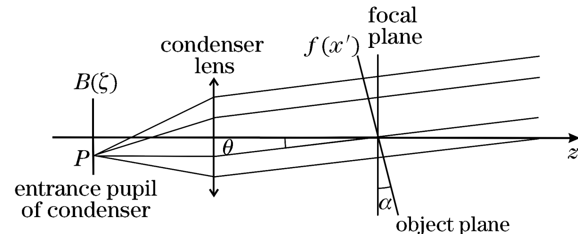

Fig. 1. Köhler illumination.

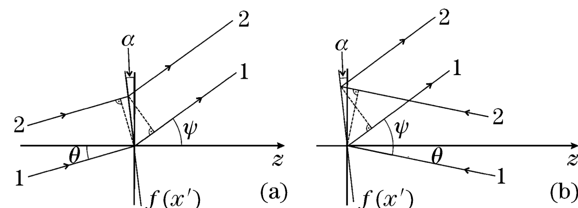

Fig. 2. Schematic to determine the phase delay of the (a) transmission or (b) reflection of the light rays at the object surface.

 © 2008 Chinese Optics Letters

may be further rewritten as

$$g(\xi',\xi)=\int_{-\infty}^{\infty}f(x')\exp[-ix'k(\xi'-\xi)]\mathrm{d}x', \qquad (4)$$

where $\xi'=\sin(\psi-\alpha)$, $\xi=\sin(\theta-\alpha)$ for the transmission type microscope and $\xi'=\sin(\psi-\alpha)$, $\xi=\sin(\theta+\alpha)$ for the reflection type microscope. If $F(u)$ represents the Fourier transform of $f(x')$, then Eq. (4) can be expressed as

$$g(\xi',\xi)=F(\frac{\xi'-\xi}{\lambda}). \qquad (5)$$

If the detector surface is vertical to the optical axis, the intensity distribution on its surface is determined by the inverse Fourier transform of $g(\xi',\xi)$. Here the frequency value relevant to $g(\xi',\xi)$ in the Fourier representation of the intensity distribution is not $(\xi'-\xi)$, but $(\sin\psi-\sin\theta)$. This becomes apparent if the reversibility of light is considered. Figure 3 shows this point. Light ray 1 impinges upon the focal plane by the angle θ and is diffracted by the angle ψ, then forms the distribution of $g(\xi',\xi)$ in the back focal plane. ξ', ξ are defined in Eq. (4) and dependent on the slant angle α. In view of the reversibility of light, the field distribution in the detector plane is assumed to be $f_{\mathrm{d}}(x,\xi_{\mathrm{d}},\alpha)$ in the case of the point source P and the slant angle α. Light ray 2 impinges upon the detector plane by the angle θ and is also diffracted by the angle ψ, then forms the same distribution of $g(\xi',\xi)$ in the back focal plane, but the frequency value relevant to $g(\xi',\xi)$ in this case should be described as $(\sin\psi-\sin\theta)$. So the complex amplitude distribution $f_{\mathrm{d}}(x,\xi_{\mathrm{d}},\alpha)$ of the detector plane is given by

$$f_{\mathrm{d}}(x,\xi_{\mathrm{d}},\alpha)=\int_{-\infty}^{\infty}g(\xi',\xi)\exp[ixk(\xi_{\mathrm{d}}'-\xi_{\mathrm{d}})]\mathrm{d}\xi_{\mathrm{d}}', \qquad (6)$$

where $\xi_{\mathrm{d}}'=\sin\psi$, $\xi_{\mathrm{d}}=\sin\theta$, and k has the same definition as in Eq. (3).

Until now we just consider the field distribution formed by light emitted from the point source P, which means that $\sin\theta$ is fixed, and the integral variable of Eq. (6) is $\sin\psi$, which is limited by the NA of the objective $\mathrm{NA_o}$. Let $B(\zeta)$ represent the brightness distribution in the entrance pupil of the condenser in one dimension, where $\zeta=\xi_{\mathrm{d}}=\sin\theta$ is limited by the NA of the condenser $\mathrm{NA_c}$. In addition, we assume that different point sources in the entrance pupil of the condenser are incoherent. In this case the overall image profile may be found by summing up the image intensities formed by all the points and is given by

$$I(x)=\int_{-\mathrm{NA_c}}^{\mathrm{NA_c}}B(\zeta)\left|f_{\mathrm{d}}(x,\xi_{\mathrm{d}},\alpha)\right|^2\mathrm{d}\zeta. \qquad (7)$$

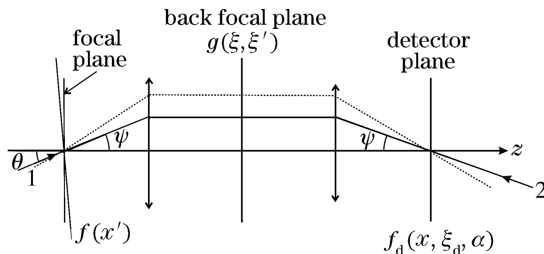

Fig. 3. Schematic sketch of light reversibility.

The complex relative transmission or reflection profile of planar objects may be written as

$$f(x')=\begin{cases}1 & |x'|<\frac{w}{2}\\ a\exp(i\Phi_1) & |x'|\geq\frac{w}{2}\end{cases}, \qquad (8)$$

where w is the linewidth, a is the relative amplitude, and Φ_1 is the relative phase change.

The periodic object approximation is a valid approximation provided that the period is large relative to the object feature. If the single line structure is replicated with spatial frequency b and offset from $x'=0$ by Δ, then the coefficient $C(u)$ of the Fourier series representation

$$f(x')=\sum_{u=-\infty}^{\infty}C(u)\exp(i2\pi ubx) \qquad (9)$$

of the line object is given by

$$C(u)=\begin{cases}bw+a(1-bw)\exp(i\Phi_1) & u=0\\ \left[\frac{1-a\exp(i\Phi_1)}{u\pi}\exp(-i2\pi\Delta ub)\right]\sin(u\pi wb) & u\neq0\end{cases}, \qquad (10)$$

where u is the index of Fourier coefficient C.

If the pupil of the condenser and the objective has only one dimension and the brightness distribution of the entrance pupil of the condenser is uniform, the overall image intensity from Eqs. (5)—(7) could be described as

$$I(x)=\sum_{n=l_1}^{l_2}\left|\sum_{m=k_1}^{k_2}C(m-n)\exp\left[i2\pi(m_{\mathrm{d}}-n_{\mathrm{d}})xb\right]\right|^2, \qquad (11)$$

where

$$l_1=-\frac{\sin(\theta_{\mathrm{NA_c}}+\alpha)}{\lambda b},\quad l_2=\frac{\sin(\theta_{\mathrm{NA_c}}-\alpha)}{\lambda b},$$

$$k_1=-\frac{\sin(\theta_{\mathrm{NA_o}}+\alpha)}{\lambda b},\quad k_2=\frac{\sin(\theta_{\mathrm{NA_o}}-\alpha)}{\lambda b},$$

$$m_{\mathrm{d}}=\frac{\sin(\Psi_m+\alpha))}{\lambda b},\quad n_{\mathrm{d}}=\frac{\sin(\theta_n+\alpha)}{\lambda b} \qquad (12)$$

for the transmission type microscope. And for the reflection type microscope, k_1 and k_2, m_{d} and n_{d} are the same as the ones in Eqs. (12) but l_1 and l_2 should be changed to

$$l_1=-\frac{\sin(\theta_{\mathrm{NA_c}}-\alpha)}{\lambda b},\quad l_2=\frac{\sin(\theta_{\mathrm{NA_c}}+\alpha)}{\lambda b}. \qquad (13)$$

In Eqs. (12) and (13), $\theta_{\mathrm{NA_o}}=\arcsin(\mathrm{NA_o})$ and $\theta_{\mathrm{NA_c}}=\arcsin(\mathrm{NA_c})$. Furthermore, $\theta_n=\arcsin(nb\lambda)$ and $\Psi_m=\arcsin(mb\lambda)$, and l_1, l_2, k_1, and k_2 are taken as the integer parts of their values respectively due to the discrete model and diffraction orders.

In our simulation, the following parameters are assumed. The linewidth $w=2$ μm, the relative amplitude $a=0$, the wavelength $\lambda=0.58$ μm, and the NAs of the objective and the condensor $\mathrm{NA_{o,c}}=0.55$. Therefore,

the coherence parameter, the ratio of NA_c to NA_o, is 1. The diffraction order taken into account depends on the selection of the frequency b of the line structures and the slant angle α. Due to the variation of the slant angle α, depending on the choice of b, the diffraction order may change as well. Therefore, the frequency b has to be chosen small enough so that the variation of the calculated profile due to a change of the diffraction order is negligible compared with the changes of the profile caused by the variation of the slant angle. It is observed that to keep the change of the calculated profile due to a variation of b smaller than 10^{-4}, b has to be chosen to $1/(1000w)$. In addition, Eq. (10) has to be divided by the number of the illumination modes $l_2 - l_1 + 1$ to obtain a normalization because the change of the slant angle leads to variation of the number of illumination modes.

Figure 4 shows the calculated image profiles of a line structure for different slant angles in the range of $0.1°-5°$ for transmission and reflection type microscopes. The profiles of reflection type microscopes can be distinguished, but the profiles for transmission type microscope cannot. Figures 5 and 6 compare the profiles of both types of microscopes for small (0.1°, 0.2° and 0.5°) and large (1°, 2°, 5°) slant angles. From these figures, it is obvious that the reflection type microscope is much stronger affected than the transmission type microscope. The maximum deviations of the profiles are about one order of magnitude smaller than those of the reflection type microscope. The maximum deviation for a slant angle of 2° reaches 0.1% in the transmission type microscope and 1% in the reflection type microscope. Furthermore, the changes of the profile in the transmission type microscope are mainly located at the edge, but the changes appear over the whole line structure in the reflection type microscope. These two figures also show that the slope at the edge of the line will change as the slant angle increases and the slant angle influences the image contrast

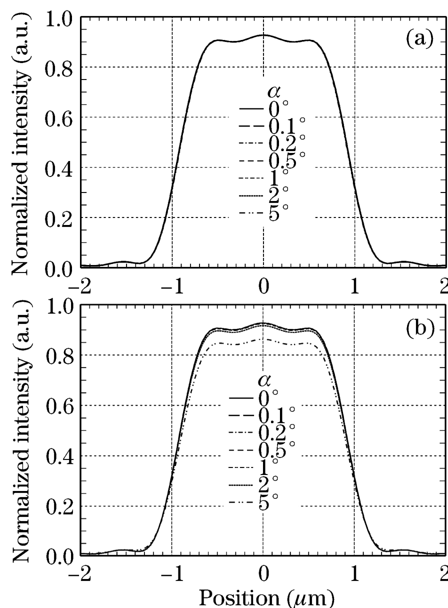

Fig. 4. Simulated intensity profiles of the 2.0-μm-wide line for different slant angles α of the (a) transmission and (b) reflection type microscopes. $NA_o = NA_c = 0.55$, $\lambda = 0.58$ μm, $b = 1/(1000w)$.

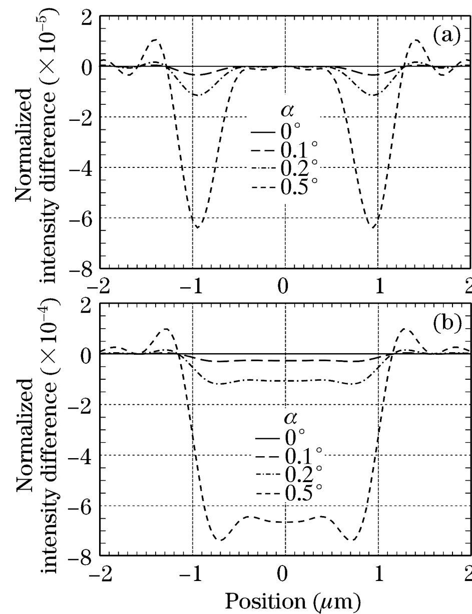

Fig. 5. Differences of the intensity profiles shown in Fig. 4 between the case of no slant angle and the cases of the slant angle $\alpha = 0.5°$, 0.2°, and 0.1° for the (a) transmission and (b) reflection type microscopes.

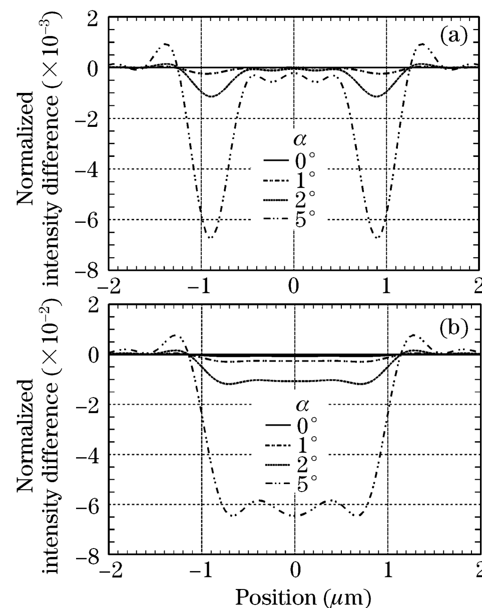

Fig. 6. Differences of the intensity profiles shown in Fig. 4 between the case of no slant angle and the cases of the slant angle $\alpha = 1°$, 2°, and 5° for the (a) transmission and (b) reflection type microscopes.

of both types microscopes differently. However, in both types of microscopes the edge slope becomes smaller if the slant angle increases. For both microscopes the image profiles seem to be symmetrical by naked eye. But exactly speaking, the slant introduces asymmetry structure image of line structure for we can see that l_1 and l_2, k_1 and k_2 are different and relevant to the slant angle from Eqs. (11)—(13). Figure 7 reveals that a large-NA objective decreases the effect of the slant angle on the shape of a line structure image.

The model is based on scalar diffraction and Fourier

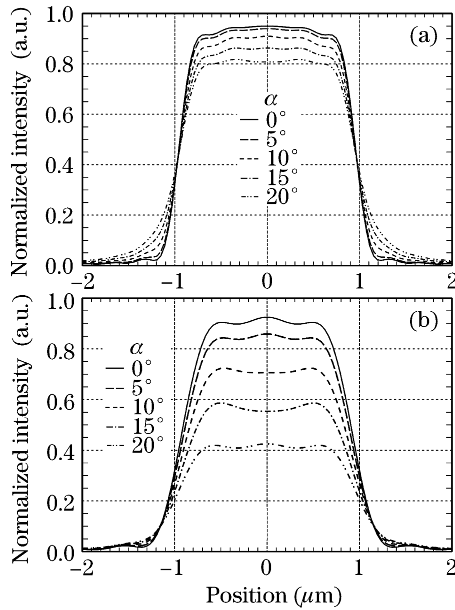

Fig. 7. Comparison of influence of slant angle α for two objectives with different NAs in the reflection type microscopes. (a) $NA_o = 0.9$; (b) $NA_o = 0.55$.

optics and the objects are assumed to be planar objects. The angle dependence of the transmission or reflection on the object surface is neglected and the optical microscope is considered to be ideal, especially its aberrations are omitted.

If the center of the observed line is not located on the optical axis and exhibits an offset Δ from the origin of the x'-axis, Eq. (9) still represents the Fourier series of this line object. In addition to a slant angle, there usually exists an amount d of defocus in the experiment, which can also be incorporated in the equation using the phase delay concept[11,12]. Then Eq. (1) should be rewritten as

$$\phi(x') = x'k\left[\sin(\theta-\alpha) - \sin(\psi-\alpha)\right] - kd\left(\cos\theta + \cos\psi\right). \tag{14}$$

And Eq. (2) is changed to

$$\phi(x') = x'k\left[\sin(\theta+\alpha) - \sin(\psi-\alpha)\right] + kd\left(\cos\theta - \cos\psi\right). \tag{15}$$

Correspondingly, Eq. (11) should become

$$I(x) = \sum_{n=l_1}^{l_2}\left|\sum_{m=k_1}^{k_2}\exp\left[\mp ikd\left(\sqrt{1-(n\lambda b)^2} \pm\sqrt{1-(m\lambda b)^2}\right)\right]C(m-n)\exp\left[i2\pi(m_{\mathrm{d}}-n_{\mathrm{d}})xb\right]\right|^2 \tag{16}$$

with the upper sign for transmission type microscope and the lower sign for reflection type microscope.

To our knowledge, the treatment of the slant angle has a general meaning in solving these kinds of problems. We conclude that the reflection type microscope is affected much more than the transmission type microscope by the slant angle. In addition, the slant angle leads to a change of the image contrast and the image shape of a line structure, especially to its edge. The larger the slant angle, the stronger the decrease of the image contrast, and the less steep the edge slope of line structures. Furthermore, the larger the NA of the objective, the less the effect of the slant angle on the line image shape.

*J. Wang was on leave from Precision Instruments Department, Tsinghua University, Beijing, P. R. China during the period of this work. Present address: Britton Chance Center for Biomedical Photonics, Huazhong University of Science and Technology, Wuhan 430074, P. R. China. His e-mail address is wangjiangang@mail.hust.edu.cn.

References

1. D. Nyyssonen, Appl. Opt. **16,** 2223 (1977).
2. D. Nyyssonen and R. D. Larrabee, J. Res. Nat. Bur. Stand. **92,** 187 (1987).
3. R. Barakat, Opt. Acta **17,** 337 (1970).
4. R. Barakat, Opt. Acta **16,** 205 (1969).
5. D. Nyyssonen, J. Opt. Soc. Am. **72,** 1425 (1982).
6. E. C. Kintner, Appl. Opt. **17,** 2747 (1978).
7. H. H. Hopkins, Photogr. Sci. Eng. **21,** 114 (1977).
8. H. H. Hopkins, J. Opt. Soc. Am. **47,** 508 (1957).
9. C. P. Kirk, "Precision measurement of microscope images" PhD Thesis (University of Leeds, 1985).
10. C. P. Kirk, Appl. Opt. **26,** 3417 (1987).
11. C.-M. Yuan, "Modeling of optical alignment and metrology in VLSI manufacturing" PhD Thesis (Carnegie-Mellon University, 1989).
12. C.-M. Yuan and A. J. Strojwas, J. Opt. Soc. Am. A **8,** 778 (1991).